Coleman, T. A., T. A. Murphy, K. R. Knupp, L. D. Carey, and M. E. Anderson, 2014: Extensive observations of the transition region of a winter storm. *J. Operational Meteor.*, **2** (1), 1–12, doi: http://dx.doi.org/10.15191/nwajom.2014.0201.

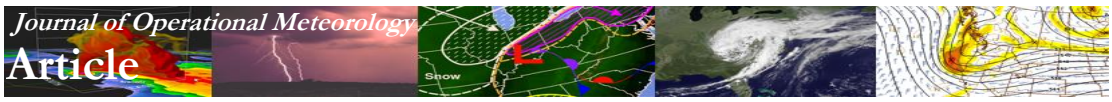

Extensive Observations of the Transition Region of a Winter Storm

TIMOTHY A. COLEMAN, TODD A. MURPHY, KEVIN R. KNUPP, and LAWRENCE D. CAREY
The University of Alabama, Huntsville, Alabama

MATTHEW E. ANDERSON
National Weather Service, Birmingham, Alabama

(Manuscript received 10 May 2013; review completed 1 November 2013)

ABSTRACT

The transition region of a winter storm affected northern Alabama on 1 February 2007, and was observed by the University of Alabama in Huntsville (UAH)/WHNT-TV Advanced Radar for Meteorological and Operational Research (ARMOR) dual-polarization C-band radar and the UAH Mobile Integrated Profiling System. This allowed for observations of the changing temperature and humidity profiles with time as precipitation transitioned from snow, to sleet, to freezing rain, and eventually to rain—as the atmosphere warmed with time. During the period of freezing rain and rain, pockets of mixed-phase precipitation continued to be observed via ARMOR, indicating the height and/or depth of the melting level varied across the area. Vertical velocity and signal-to-noise ratio data from the wind profiler also are examined as precipitation type changed. The observations allow for explanation of the large-scale and microphysical processes occurring in this transition region.

1. Introduction

Northern Alabama receives, on average, two days of measurable snowfall each year (NWS 2013), with many of these exhibiting transitions in precipitation type and/or mixed precipitation. Because of the infrastructure in Alabama, even a small accumulation of snow, sleet, or freezing rain on road surfaces often causes significant economic impacts. Transitional and mixed-phase events exacerbate this problem, since local National Weather Service (NWS) Weather Forecast Offices and emergency managers must rely on public reports and surface observations as to when and where winter precipitation is occurring. It often is difficult to locate mixed-phase precipitation using single plan position indicator scans of reflectivity factor at horizontal polarization (Z_H) from traditional horizontally polarized radars. Radar bright-band detection (Austin and Bemis 1950; Fabry and Zawadzki 1995; Gourley and Calvert 2003) has offered the best method for discerning precipitation type with horizontally polarized radars through identification of the melting layer (Marwitz and Toth 1993). However, using the bright band presents some limitations in discerning precipitation type. For example, a reflectivity bright band can be associated with partially melted aggregates due to an increase in the dielectric constant (NCAR 2013). Depending on the thermodynamic profile, partially melted aggregates can refreeze and then melt again, causing a double bright band (Ikeda et al. 2005). As will be suggested herein, partially melted aggregates beneath a reflectivity bright band also can extend to the ground.

For real-time observations, dual-polarization radar observations have improved the ability to identify hydrometeor type as well as the melting layer. Polarimetric measurements such as differential reflectivity (Z_{DR}) and correlation coefficient (ρ_{hv}) exhibit well-pronounced signatures within regions of mixed-phase precipitation and across melting layers (Zrnić et al. 1993; Brandes and Ikeda 2004). Herzegh and Jameson (1992) showed how Z_{DR} changes across the melting level, suggesting values near 0–1 dB for low-density aggregates above the melting level, but a drastic increase to 3–4 dB as hydrometeors fall into air that is above freezing and begin to melt. Ryzhkov and

Corresponding author address: Dr. Timothy A. Coleman, The University of Alabama, 320 Sparkman Drive, Huntsville, AL 35899
E-mail: coleman@nsstc.uah.edu

Zrnić (1998) found a similar Z_{DR} structure within melting layers, in addition to a minimum in ρ_{hv} at the bottom of melting layers. In aggregates above and rain below the melting layer, ρ_{hv} typically is >0.95. In areas of mixed hydrometeors, ρ_{hv} typically is <0.95 and >0.70, but can be as low as 0.50 (Straka et al. 2000). Generally, 0.80 is the lowest value of ρ_{hv} observed for meteorological echoes, according to the NWS and other sources (e.g., radarscope.tv/faqs/correlation-coefficient-cc/). Although ρ_{hv} is near 1.0 in snow aggregates, ρ_{hv} may decrease if any liquid water also is present. For example, partially melted aggregates beneath a bright band are associated with lowered ρ_{hv} (Ikeda et al. 2005), providing additional information beyond reflectivity regarding hydrometeor state.

Regarding the part of winter storms where sudden changes in precipitation type are occurring, relatively few fine-scale temporal and spatial observations of the temperature, pressure, and geopotential height profiles are available in the literature In these transition regions, many competing synoptic and microphysical processes may be occurring, making temperature and precipitation-type forecasts difficult. Warm or cold advection may be occurring. Latent heating due to freezing—and latent cooling due to melting, evaporation, and sublimation (e.g., Market et al. 2006)—may play a significant role in atmospheric temperature changes. Also, some heating and cooling may occur simply because of the transport of heat (or a heat deficit) by the fall of hydrometeors into a layer that has a different temperature than the hydrometeors themselves, although quantitative studies on this process are lacking.

In this paper, we examine a winter storm that affected the southeastern United States on 1 February 2007. The entire precipitation transition region moved across Huntsville, Alabama, with precipitation transitioning from snow through sleet, freezing rain, and then ending as rain. One-minute resolution observations of the atmospheric temperature profile, approximate precipitation fall speed, and 1000–850-mb thickness (e.g., Stewart and King 1987) are presented. Additionally, this study will display the utility of polarimetric observations during mixed-phase precipitation events, which is becoming increasingly important for operational forecasters with the dual-polarization upgrade to the Weather Surveillance Radar-1988 Doppler (WSR-88D) radar network. The microphysical processes occurring in this transition in precipitation type are discussed, and the thicknesses of the midlevel melting layer and near-surface refreezing layer (for sleet and freezing rain) are examined. It is shown that, in a saturated atmosphere, a relatively shallow layer of air just above freezing is still sufficient to melt snow, producing sleet or rain at the surface. Temperature changes due to latent heating are illustrated.

2. Data collection and methods

The primary data sources for this study are the Advanced Radar for Meteorological and Operational Research (ARMOR) dual-polarization radar (Peterson et al. 2005), as well as a microwave profiling radiometer (MPR) and a 915-MHz Doppler wind profiler—both part of the University of Alabama in Huntsville (UAH) Mobile Integrated Profiling System (MIPS; Karan and Knupp 2006). A particle size velocity (PARSIVEL) disdrometer (Löffler-Mang and Joss 2000) also was running at the MIPS site, providing some information on precipitation type as well as 1-min averages of precipitation rate. MIPS was located on the campus of UAH during this storm. Other measurements were used, including various surface meteorological instrumentation across the region [specifically at the Huntsville airport (KHSV) and at the University of Alabama in Huntsville (KUAH)]. Additional analyses from the Storm Prediction Center (SPC) mesoscale analysis webpage (www.spc.noaa.gov/exper/mesoanalysis/), and analyses from the Plymouth State University archive webpage—that uses archived upper-air data and WXP software (refer to vortex.plymouth.edu/ua-u.html and wxp.unisys.com/)—are used to illustrate synoptic-scale features.

The ARMOR is a fixed-site, C-band dual-polarization scanning radar with a 1° beamwidth. ARMOR data have been utilized in other studies (e.g., Deierling and Petersen 2008; Anderson et al. 2011; Thurai et al. 2012). There are three primary ARMOR variables analyzed in this study. One is the previously defined Z_H. Another that measures particle oblateness is Z_{DR}, defined as the ratio of Z_H and the reflectivity factor at vertical polarization (Z_V). Z_{DR} is reflectivity weighted, which means that strongly reflective targets will contribute more to Z_{DR} than weakly reflective targets. The third is ρ_{hv}, a measure of the similarity between the horizontal and vertical returns. For example, in stratiform rain, all drops are nearly spherical, resulting in a ρ_{hv} near 1.0. For meteorological returns, ρ_{hv} typically is >0.7 at C- and S-bands (Bringi and Chandrasekar 2001).

Even in light to moderate precipitation, the MPR provides accurate vertical profiles of temperature and water vapor in the lowest 2 km AGL. However, there are some errors in MPR measurements, just as there are in radiosonde measurements (e.g., Güldner and Spänkuch 2001; Knupp et al. 2009). In this experiment, the 0°C level was estimated at a given time based on the rapid downward acceleration of precipitation (shown in MIPS profiler measurements of vertical motion). The bias of the MPR temperature measurements at that level was then computed and interpolated to the surface, assuming zero error at the surface. Given the pressure at the surface, an iterative technique using the hydrostatic equation may be used to produce a vertical profile of geopotential height and, therefore, a fairly accurate time series of the 1000–850-mb thickness. Surface observations from the PARSIVEL disdrometer, in combination with the automated surface observation station at KHSV, were used to determine precipitation type at UAH. KHSV is only 16 km west-southwest of UAH, and given that the frontal boundary and associated isotherms were oriented roughly west-to-east in this system, the precipitation types at KHSV and UAH presumably were the same, especially over large time scales (i.e., >5 min).

3. Analysis

At 0600 UTC 1 February 2007, a stationary front and associated pressure trough were located near the Gulf Coast (Fig. 1a). Upstream, a large-scale and deep upper-level trough axis was located over the southwestern United States and was translating eastward while amplifying (Fig. 1b). Ahead of this trough, height falls at 850 mb were evident in association with 300-mb divergence observed over Mississippi and Alabama; these height falls likely were also due to the development of widespread precipitation and latent heat release. The low-level height falls were associated with southerly flow and warm advection at 850 mb over Alabama (Fig. 2). Streamline analysis of the flow indicates that the warm advection above the surface had already begun at 0000 UTC. There was almost no thermal advection near the surface at the MIPS location (Fig. 3a), but fairly significant warm advection at 925 mb (Fig. 3b) and 850 mb (not shown for 0000 UTC). The isentropic lift associated with this low-level warm advection, and convergence associated with surface pressure falls, produced widespread precipitation over northern Alabama.

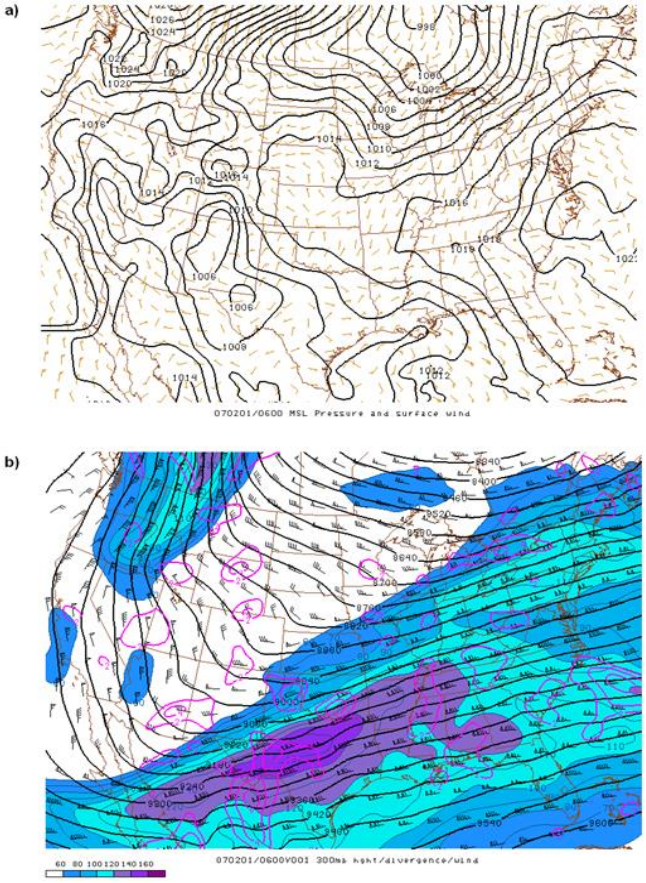

Figure 1. (a) Mean sea level pressure (solid) and surface wind barbs at 0600 UTC 1 February 2007. (b) 300-mb heights (solid black), winds (shaded isotachs in kt, and barbs), and divergence (positive values in purple contours) at same time. Images from the SPC (www.spc.noaa.gov/exper/ma_archive/). *Click image for an external version; this applies to all figures hereafter.*

a. Precipitation onset and cooling

The radar composite loop starting at 0311 UTC, and containing roughly one image per hour through 1108 UTC, is shown in Fig. 4. The radar shows precipitation overspreading northern Alabama by 0400 UTC, but precipitation did not begin at the ground until 0535 UTC (Fig. 5). The surface temperature and dewpoint plots at UAH (Fig. 6) indicate that the air was initially very dry at the surface when precipitation began to appear on radar at 0400 UTC. Precipitation began as all snow around 0530 UTC, and temperatures at the surface dropped quickly from 1.5°C (35°F) to –1°C (30°F) in 1.5 h. At the same time, the dewpoint quickly rose to near the temperature. Since wet snow was falling, this decrease in temperature and increase in dewpoint was almost entirely produced by evaporational and sublimational cooling (e.g., Market et al. 2006)—the cooling that occurs when ice transitions

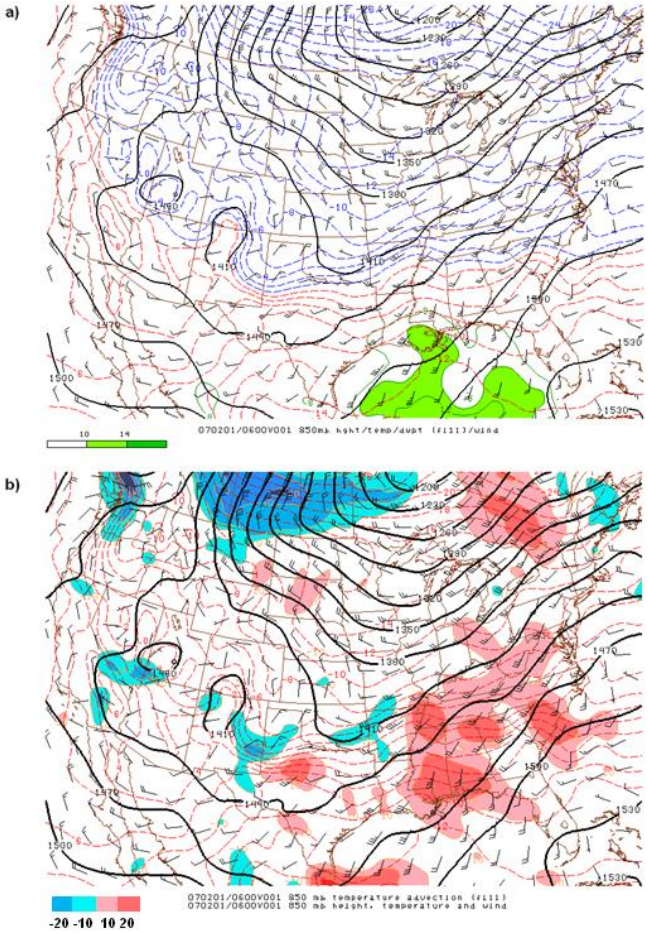

Figure 2. (a) Heights (m, solid), temperatures (°C, dashed), wind barbs, and dewpoint (°C, fill) at 850 mb at 0600 UTC 1 February 2007; (b) Heights (m, solid), temperatures (°C, dashed), wind barbs, and temperature advection (10^{-5} °C s^{-1}, fill) at same time. Images from the SPC (www.spc.noaa.gov/exper/ma_archive/).

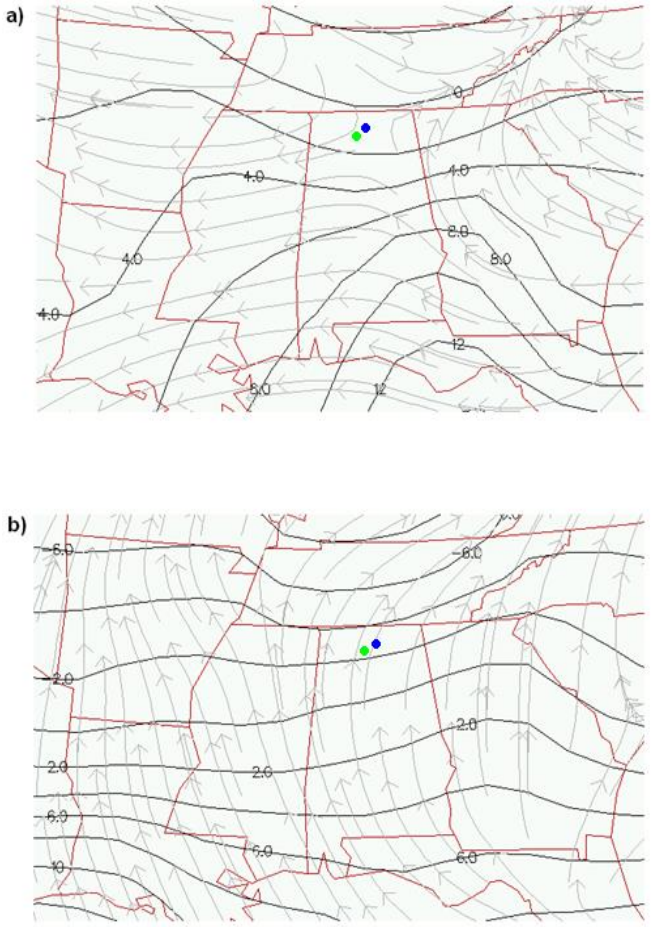

Figure 3. Streamline analysis of wind flow (gray arrows) and temperature (°C, black contours) at (a) 1000 mb and (b) 925 mb, at 0000 UTC 1 February 2007. Blue dot shows approximate location of MIPS, and green dot shows approximate location of ARMOR. Images from Plymouth State University (vortex.plymouth.edu/ua-u.html).

directly to the vapor phase. MPR data indicated that the saturated layer where precipitation was likely forming extended from 1 to 4.5 km AGL at 0530 UTC, and temperatures were less than –6°C above 2.5 km AGL, and as low as –16°C in this layer. These temperatures are cold enough for ice crystal formation (e.g., MetEd 2013; WDTB 2013).

The erosion of the low-level dry air and the simultaneous cooling are illustrated by the MPR time-height sections of temperature and relative humidity (RH, Fig. 7) and by the 915-MHz wind profiler signal-to-noise ratio (SNR). Note that the air initially was drier throughout the lowest 300 m AGL, then after 0535 UTC the air began to become saturated closer to the ground. Precipitation began at 0534 UTC. Notice also that the drop in temperature at low levels occurs from the top down, indicating that the virga was falling and sublimating, causing cooling and

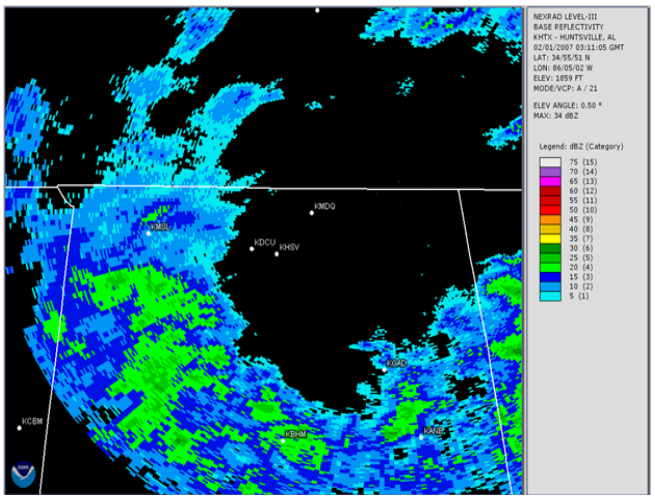

Figure 4. Radar reflectivity (dBZ) from the WSR-88D at KHTX valid 0311 UTC 1 February 2007. *Click image for an external animation valid 0311–1108 UTC 1 February 2007.*

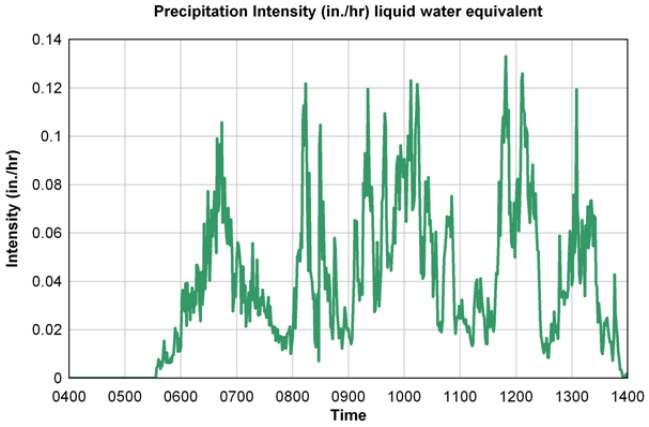

Figure 5. Liquid equivalent precipitation intensity (in h^{-1}) as measured by the PARSIVEL disdrometer at the MIPS site from 0400 through 1400 UTC on 1 February 2007.

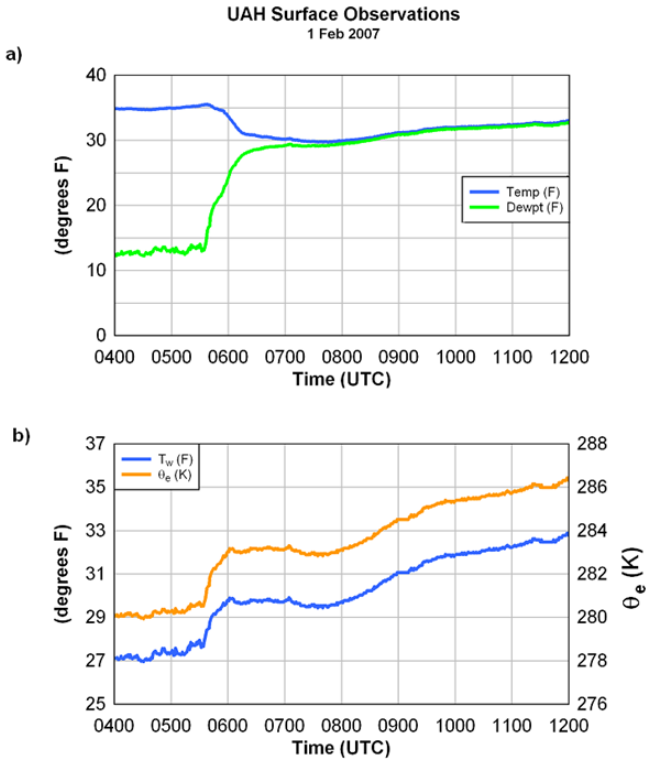

Figure 6. (a) Time series of surface temperature (blue, °F) and dewpoint (green, °F) at the UAH MIPS location from 0400 to 1200 UTC on 1 February 2007. (b) Time series of surface wet bulb temperature (blue, °F) and θ_e (orange, K) for same times.

increasing the RH at lower levels with time. The increasing RH allowed precipitation to fall through a deeper saturated layer until it was finally able to reach the surface. The increasing SNR data from the 915-MHz profiler (Fig. 8a) at lower elevations with time indicate the descent of the sublimation level (where most falling precipitation was drying up) between

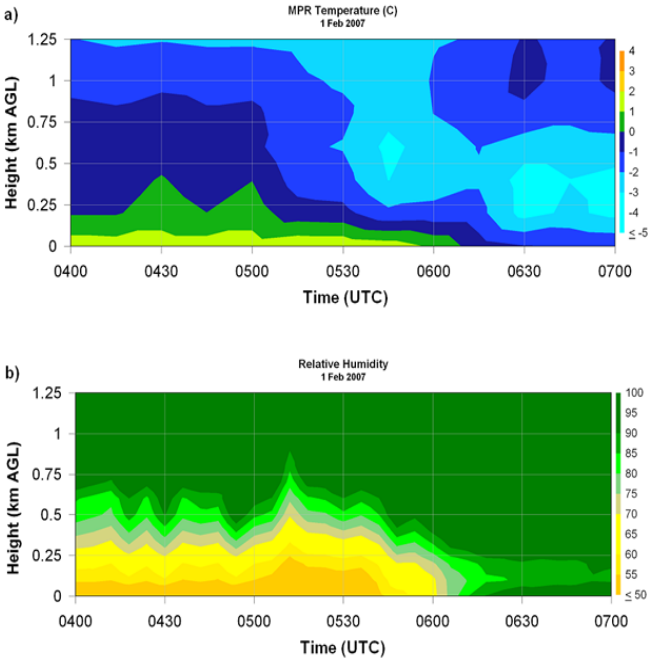

Figure 7. (a) Time-height section of temperature (°C) from the MPR at UAH on 1 February 2007. (b) Similar to (a), except for RH (percent).

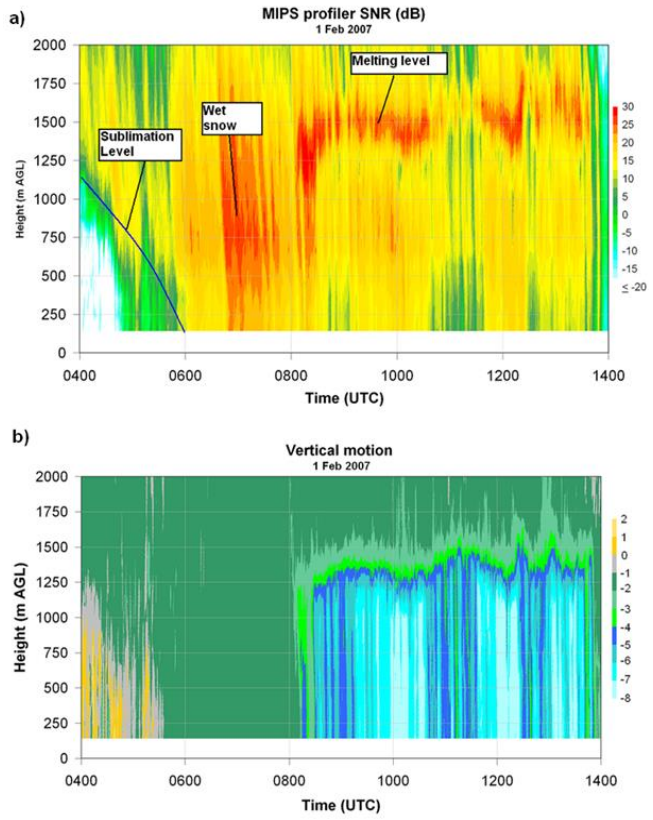

Figure 8. Time-height section of (a) wind profiler signal-to-noise ratio (dB), and (b) wind profiler Doppler vertical velocity W (m s^{-1}), from MIPS on 1 February 2007. Downward motion is negative.

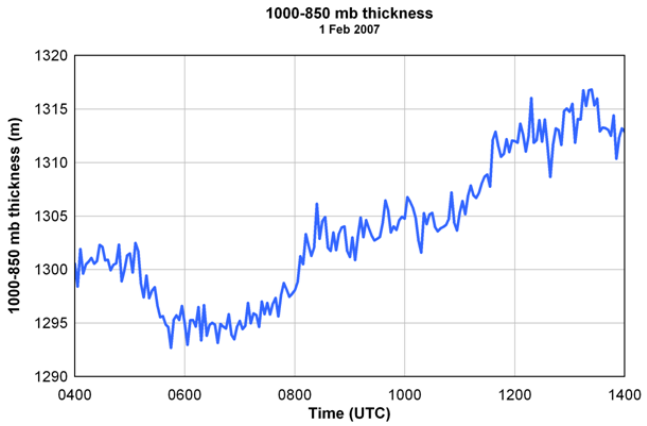

Figure 9. Time series of MPR-derived 1000–850-mb thickness (m) on 1 February 2007.

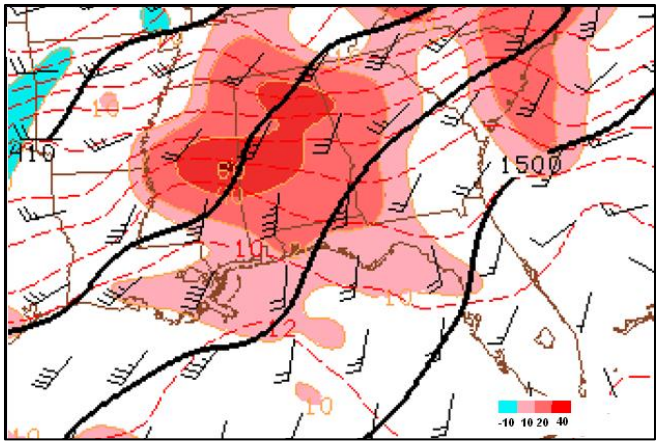

Figure 10. 850-mb heights (m, black contours), temperatures (°C, dashed contours), wind barbs, and temperature advection (shading, 10^{-5} °C s^{-1}) at 0800 UTC 1 February 2007.

0400 and 0600 UTC. The overall cooling of the lowest 500 m AGL is indicated by a decrease in the 1000–850-mb thickness (Fig. 9), which fell from 1302 m at 0500 UTC to 1293 m just after 0600 UTC.

b. Warm advection aloft and transition to sleet

After 0730 UTC, warm advection above the 500-m AGL layer began to have a significant impact on temperatures. Warm advection increased at 850 mb between 0600 and 1200 UTC (Fig. 10), but it had been occurring since well before 0600 UTC. Microphysical processes, including sublimation, likely offset most of the warm advection until around 0730 UTC, when temperatures began to warm in the 500–1500-m AGL layer. The 1000–850-mb thickness increased from 1297 m at 0730 UTC to 1304 m by 0830 UTC (Fig. 9). Figure 11, perhaps the most illustrative figure in this paper, shows a time-height section of temperatures from 0400 to 1400 UTC 1 February 2007, along with a timeline of precipitation types falling at KHSV during that period. Temperatures at 1000 m AGL increased from –1.3°C at 0600 UTC to above 0°C by 0800 UTC. Due to warm advection, a layer of air 900-m deep, centered near 1200 m AGL, was above freezing by 0825 UTC. The warm advection above 500 m AGL is very apparent in Fig. 11.

Surface observations at KHSV indicated that sleet began to mix with snow at 0810 UTC, then the precipitation became all sleet by 0815 UTC. The sleet indicates that the layer of air only 900-m deep, at temperatures between 0 and 1.3°C, was able to at least partially melt the falling snow. The depth and temperature of a layer and its ability to melt precipitation is governed partially by the size of the ice particles falling into the layer. Larger ice particles require a warmer and/or a deeper melting layer. This process was evaluated by Czys et al. (1996). However, the maximum temperature of 1.3°C in the warm layer, above a freezing surface layer, is consistent with sleet, as shown in the top-down process to determine precipitation type (e.g., MetEd 2013; WDTB 2013). The layer of air at low levels that resulted in refreezing of hydrometeors into sleet contained temperatures mainly between –1 and –2°C, much warmer than that indicated for refreezing of raindrops into sleet (e.g., MetEd 2013; WDTB 2013). Thus, the snowflakes likely only partially melted in the warm layer between 0.7 and 1.6 km AGL, leaving an inner core of ice, making ice nucleation in the low-level cold layer more likely.

It should be noted that the layer of air with a temperature primarily between 0 and 1°C that moved in around 0800 UTC warmed very little for a significant period of time. Only part of the layer exceeded 1°C for a short period of time between 0800 and 0945 UTC, despite the warm advection. This is shown by the fairly constant 1000–850-mb thickness in this layer between 0830 and 0945 UTC near 1303 m, after the sudden increase between 0700 and 0830 UTC (Fig. 9). This is likely due to the cooling associated with melting of snow in this layer. However, the layer of air between 0 and –2°C below 700 m AGL was sufficient to refreeze the partially melted snowflakes into sleet.

The transition also is shown in the time-height section of W (Doppler velocity, $W = w + V_t$, where w is vertical air motion and V_t is the terminal fall speed of the hydrometeors) from the MIPS profiler (Fig. 8b).

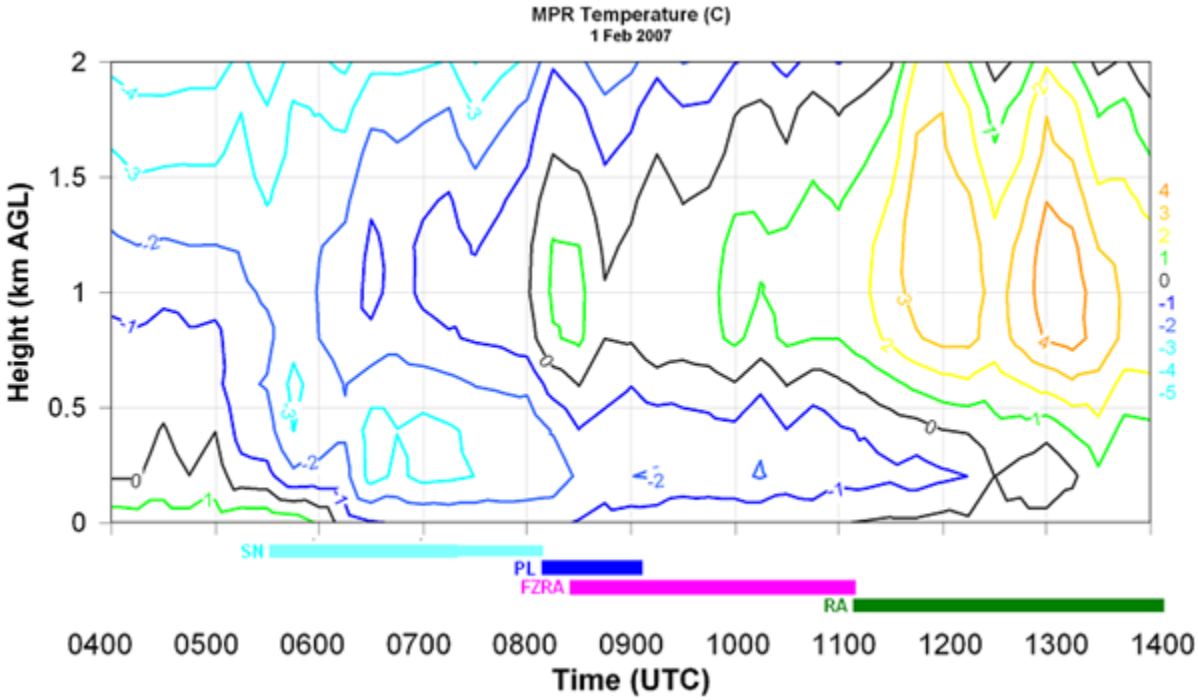

Figure 11. Time-height section of temperature (°C) from MPR on 1 February 2007. Precipitation types snow (SN), sleet (PL), freezing rain (FZRA), and rain (RA) shown with respect to time, from 5-min observations at KHSV and PARSIVEL disdrometer observations.

The typical terminal fall speed for snowflakes at temperatures between 0 and –3°C is about 1 m s^{-1} (e.g., Geerts 2013; Brandes et al. 2007), and average *W* at 500 m AGL was about 1.5 m s^{-1} between 0600 and 0800 UTC. Given the inversion height of about 700 m AGL in this case, and based on Crawford and Stewart (1995) and data from Locatelli and Hobbs (1974), the terminal fall speeds for ice pellets should be somewhat higher, between 1 and 3 m s^{-1}. Note that downward *W* begins to increase with the transition to sleet by around 0815 UTC (Figs. 8b and 11), and by 0820 UTC, *W* at 500 m AGL was 3.8 m s^{-1}. A thorough discussion of the operational meteorology top-down precipitation type technique should be examined (e.g., MetEd 2013; WDTB 2013).

c. Transition to freezing rain

Freezing rain began to mix with the sleet at 0825 UTC. Sleet continued through 0905 UTC, but at 0910 UTC, all precipitation at the ground was in the form of freezing rain. This transition was due to the continued warming with time between 700 and 1500 m AGL, especially after 0900 UTC (Fig. 11), owing to warm advection. After 0900 UTC, the MPR shows a slow warming of the layer below 700 m AGL (Fig. 11). The transition with time to more freezing rain than sleet may be inferred from the increasing downward vertical velocities in Fig. 8b. At 0825 UTC, when freezing rain began to mix with the sleet, average hydrometeor vertical velocities at 500 m AGL were 2.7 m s^{-1}. By 0900 UTC, fall velocities had increased to 4.5 m s^{-1}, and at 0930 UTC, with only freezing rain falling, fall velocities were 5.7 m s^{-1}, typical of raindrops. Freezing rain fell at KHSV from 0910 through 1105 UTC. Surface (2 m AGL) temperatures slowly rose from –0.4°C (31.2°F) to 0.2°C (32.4°F) during the time that freezing rain was occurring (Figs. 6a and 11), even though the raindrops were falling through a significant layer of cold air (between 0 and –2°C) that extended up to 500 m AGL until about 1130 UTC.

d. Transition to rain

As warm advection continued at low levels, the layer of sub-freezing air became shallower with time between 0900 and 1100 UTC, and by 1110 UTC, temperatures at the surface went above freezing (Figs. 6a and 11). At this time, the freezing rain transitioned to rain, even though melting of the layer of snow and ice on the ground would have tended to slow any warming in the atmosphere as temperatures began to rise above freezing. When surface temperatures rose above 0°C, the layer of air above 0°C aloft was about

1100-m deep. A layer of air below 0°C continued above the surface through 1315 UTC, but it clearly was not deep enough to supercool any of the falling raindrops to the point where they would freeze on impact with the surface.

e. Heterogeneity in the rain and freezing rain area

During the period when rain and freezing rain were reported across northern Alabama, polarimetric observations suggested some locations were likely still experiencing mixed-phase precipitation, indicating a melting level that was not completely uniform across northern Alabama, and/or larger particles not fully melting before reaching the surface. As an example of this, Fig. 12 shows attenuation-corrected Z_H (CZ_H), Z_{DR}, and ρ_{hv} at 0955 UTC, when freezing rain was occurring at KHSV and KUAH. The radar shows ρ_{hv} near 0.99 out to a range of 45 km (Fig. 12c), indicating fairly uniform precipitation (rain) in this area. However, an area of relatively high CZ_H (>35 dBZ; outlined by the black box in Fig. 12a) was collocated with ρ_{hv} ≤0.93 and Z_{DR} ≥3 dB (Fig. 13). These observations indicate this area is a region of mixed-phase hydrometeors, likely including a mixture of aggregates, partially melted aggregates, and rain.

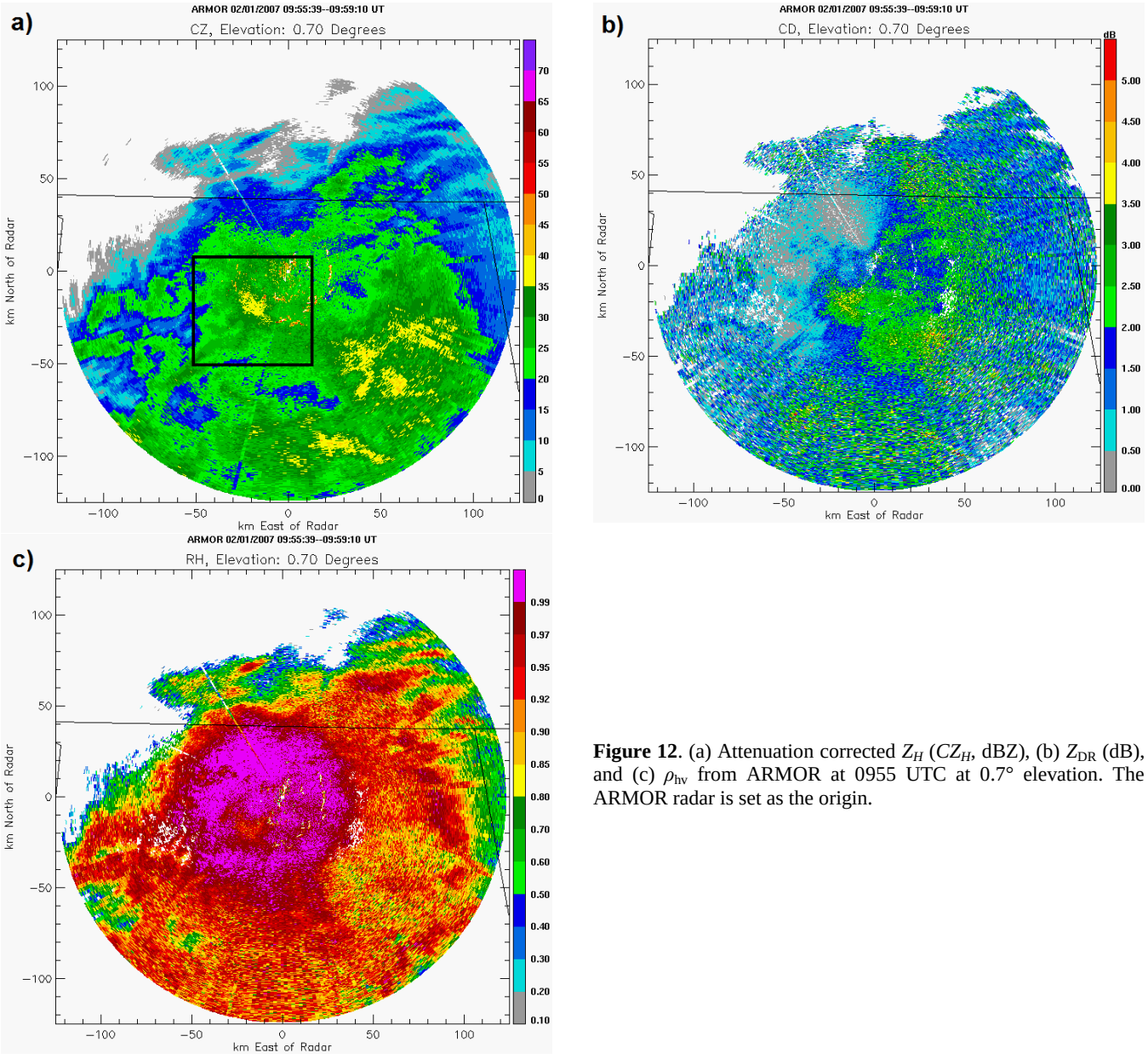

Figure 12. (a) Attenuation corrected Z_H (CZ_H, dBZ), (b) Z_{DR} (dB), and (c) ρ_{hv} from ARMOR at 0955 UTC at 0.7° elevation. The ARMOR radar is set as the origin.

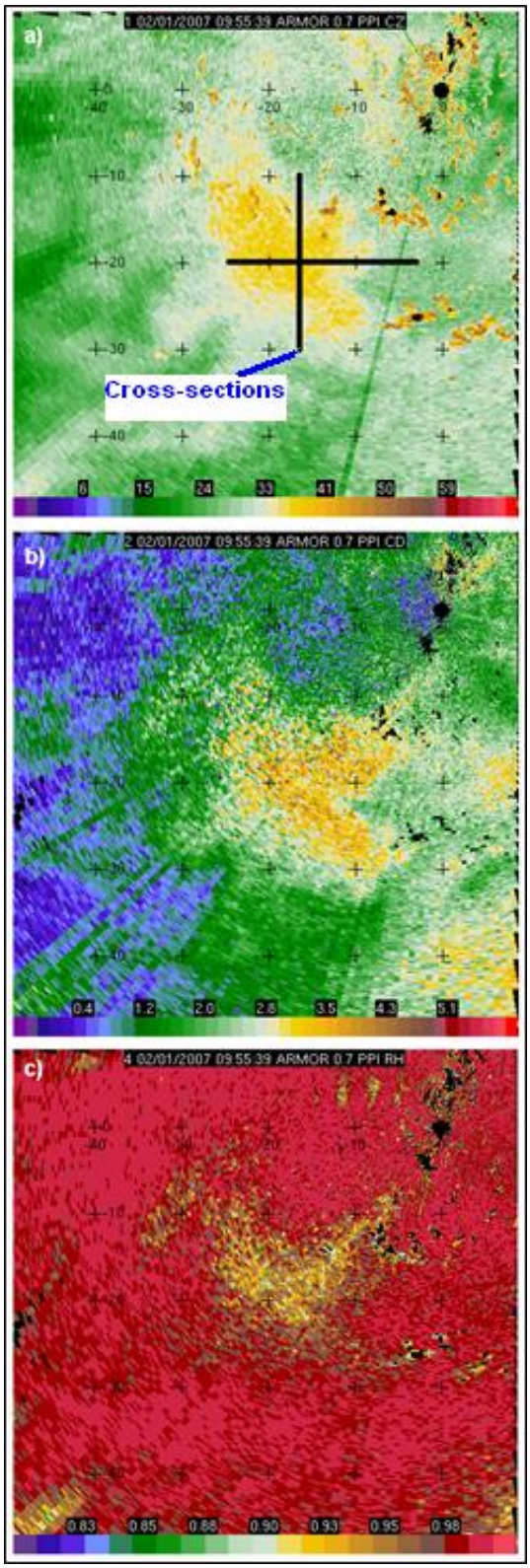

Figure 13. ARMOR data at 0955 UTC centered on the area outlined in Fig. 12a. (a) CZ_H (dBZ); (b) Z_{DR} (dB); and (c) ρ_{hv}. Tick marks are included every 10 km. The black lines in panel (a) indicate approximate locations of vertical cross sections in Figs. 14 and 15.

To further examine this area, east–west (Fig. 14) and north–south (Fig. 15) cross sections of gridded radar data were taken along the two lines shown in Fig. 13a. In both cross sections (Figs. 14 and 15), CZ_H begins increasing slightly above the MPR-observed melting level. The increase in CZ_H, combined with the increase in Z_{DR} near the same height, indicates an increase in particle size due to aggregation as the environmental temperature increases to near 0°C. CZ_H maximizes at or just above the melting level as indicated by the MPR. This is the radar "bright band," where melting, water-coated ice particles produce large values of radar reflectivity. There are also clear indications of melting via the polarimetric variables. According to Ryzhkov and Zrnić (1998), the radar bright band exhibits a positive peak in Z_{DR} at the bottom of the melting level with a minimum in ρ_{hv} at or just below the melting level, where a transition from ice particles to mixed phase occurs. Figures 14 and 15 both show Z_{DR} reaching a maximum below the melting level. More importantly, a ρ_{hv} minimum is located near 1.5 km AGL, indicating a mixture of rain and ice particles or partially melted aggregates. The radar-perceived location of the melting level appears at a similar height as that observed by the MPR. One interesting feature in Figs. 14 and 15 are the areas of $\rho_{hv} \leq 0.95$ extending from the melting level toward the surface—specifically centered around x = –15 to –20 km in Fig. 14 and y = –15 to –20 km in Fig. 15. This ρ_{hv} lowering suggests mixed-phase hydrometeors may be reaching the surface near these locations.

4. Summary

The transition region of a winter storm, including all four major types of winter precipitation (snow, sleet, freezing rain, and rain), was well-sampled by the MIPS instrumentation at UAH and by the ARMOR radar on 1 February 2007. The precipitation was associated with warm advection aloft, primarily between 500 and 1500 m AGL.

Several of the microphysical processes that occur in these transition regions were illustrated well by the microwave profiling radiometer and the 915-MHz wind profiler. Snow initially fell into dry air near the surface, causing sublimation and resulting in cooling and moistening. With the increase in RH, snow eventually reached the ground. Sustained warm advection above 500 m AGL eventually caused a layer of air above 0°C (a melting layer) at Huntsville. Dual-polarization radar interpretation of the melting level

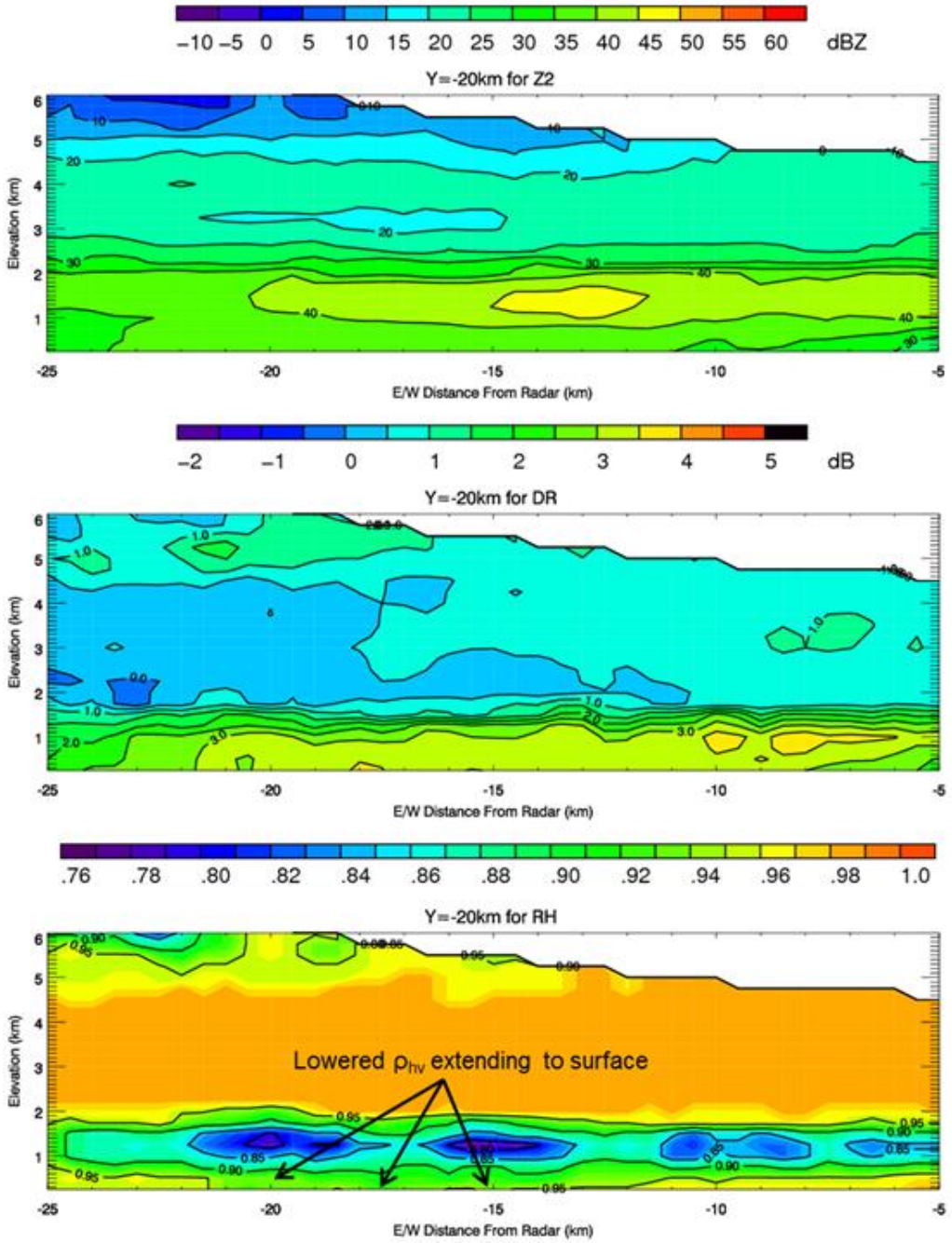

Figure 14. West–east vertical cross sections of CZ_H (dBZ; top), Z_{DR} (dB; middle), and ρ_{hv} (bottom) at y = –20 km.

was fairly consistent with that observed in the MPR data. Snowflakes melted, as shown by a bright band in profiler SNR data and an increase in downward velocity. As shown by the MPR, this melting layer remained primarily between 0 and –1°C for almost two hours, due to the absorption of heat by melting of snow, and 1000–850-mb thicknesses remained fairly constant for a period of time despite warm advection.

The layer of cold air below 500 m AGL allowed for refreezing of the melted snow into sleet for about one hour, but the freezing process allowed the low-level cold layer to warm somewhat with time, and the precipitation transitioned to freezing rain, as surface temperatures remained ≤0°C. Profiler measurements illustrate the increase in downward vertical velocities with time, as the precipitation aloft transitioned from

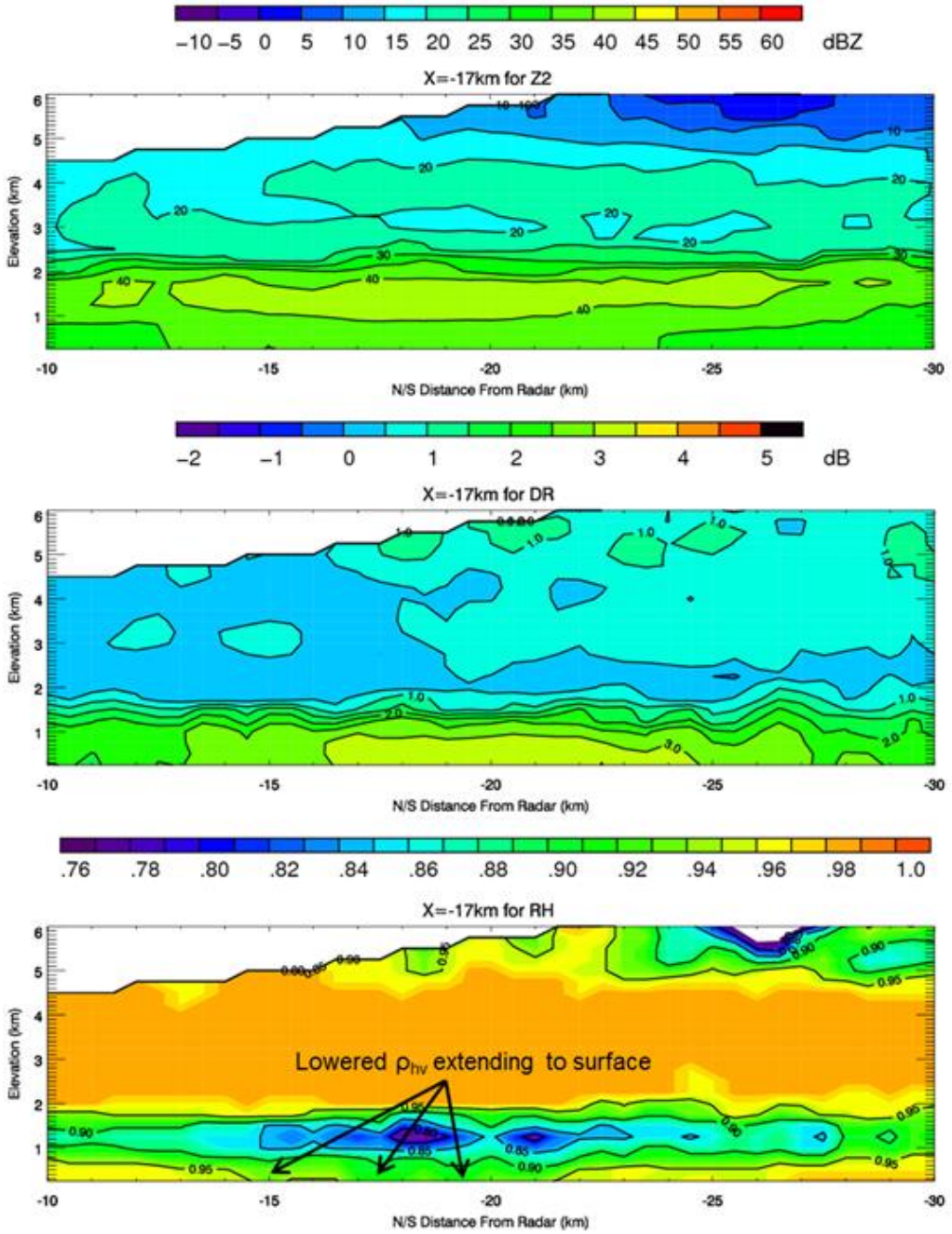

Figure 15. Same as Fig. 14 but a north–south cross section at x = –17 km.

snow to sleet to rain. However, there were areas of lowered ρ_{hv} extending from the melting level to the surface, suggesting mixed-phase particles (i.e., aggregates of snowflakes, partially melted aggregates, and rain) reaching the surface in isolated areas.

Air continued to warm aloft owing to advection. Surface temperatures rose above 0°C, and freezing rain transitioned to rain. The process was slow, however, as snow and ice already on the ground began to melt.

The time-height sections of temperature from the MPR illustrate the transition region in the winter storm well, and vertical velocity and SNR measurements from the wind profiler add further insight to this case. Forecasters must be aware of the often offsetting microphysical processes when portions of the atmosphere are near 0°C.

Acknowledgments. The authors thank Dustin Phillips, Chris Phillips, and Adam Sherrer for their assistance with the UAH MIPS system and data retrieval. We also thank the reviewers, whose comments improved the manuscript.

REFERENCES

Anderson, M. E., L. D. Carey, W. A. Petersen, and K. R. Knupp, 2011: C-band dual-polarimetric radar signatures of hail. *Electronic J. Operational Meteor.*, **12** (2), 1–30.

Austin, P. M., and A. C. Bemis, 1950: A quantitative study of the "bright band" in radar precipitation echoes. *J. Meteor.*, **7**, 145–151.

Brandes, E. A., and K. Ikeda, 2004: Freezing-level estimation with polarimetric radar. *J. Appl. Meteor.*, **43**, 1541–1553.

____, K. Ikeda, G. Zhang, M. Schönhuber, and R. M. Rasmussen, 2007: A statistical and physical description of hydrometeor distributions in Colorado snowstorms using a video disdrometer. *J. Appl. Meteor. Climatol.*, **46**, 634–650.

Bringi, V. N., and V. Chandrasekar, 2001: *Polarimetric Doppler Weather Radar: Principles and Applications*. Cambridge University Press, 636 pp.

Crawford, R. W., and R. E. Stewart, 1995: Precipitation type characteristics at the surface in winter storms. *Cold Reg. Sci. Technol.*, **23**, 215–229.

Czys, R. R., R. W. Scott, K. C. Tang, R. W. Przybylinski, and M. E. Sabones, 1996: A physically based, nondimensional parameter for discriminating between locations of freezing rain and ice pellets. *Wea. Forecasting*, **11**, 591–598.

Deierling, W., and W. A. Petersen, 2008: Total lightning activity as an indicator of updraft characteristics. *J. Geophys. Res.*, **113**, D16210, doi:10.1029/2007JD009598.

Fabry, F., and I. Zawadzki, 1995: Long-term radar observations of the melting layer of precipitation and their interpretation. *J. Atmos. Sci.*, **52**, 838–851.

Geerts, B., cited 2013: Fall speed of hydrometeors. [Available online at www-das.uwyo.edu/~geerts/cwx/notes/chap09/hydrometeor.html.]

Gourley, J. J., and C. M. Calvert, 2003: Automated detection of the bright band using WSR-88D data. *Wea. Forecasting*, **18**, 585–599.

Güldner, J., and D. Spänkuch, 2001: Remote sensing of the thermodynamic state of the atmospheric boundary layer by ground-based microwave radiometry. *J. Atmos. Oceanic Technol.*, **18**, 925–933.

Herzegh, P. H., and A. R. Jameson, 1992: Observing precipitation through dual-polarization radar measurements. *Bull. Amer. Meteor. Soc.*, **73**, 1365–1374.

Ikeda, K., E. A. Brandes, and R. M. Rasmussen, 2005: Polarimetric radar observations of multiple freezing levels. *J. Atmos. Sci.*, **62**, 3624–3636.

Karan, H., and K. Knupp, 2006: Mobile Integrated Profiler System (MIPS) observations of low-level convergent boundaries during IHOP. *Mon. Wea. Rev.*, **134**, 92–112.

Knupp, K. R., R. Ware, D. Cimini, F. Vandenberghe, J. Vivekanandan, E. Westwater, T. Coleman, and D. Phillips, 2009: Ground-based passive microwave profiling during dynamic weather conditions. *J. Atmos. Oceanic. Tech.*, **26**, 1057–1073.

Locatelli, J. D., and P. V. Hobbs, 1974: Fall speeds and masses of solid precipitation particles. *J. Geophys. Res.*, **78**, 3619–3620.

Löffler-Mang, M., and J. Joss, 2000: An optical disdrometer for measuring size and velocity of hydrometeors. *J. Atmos. Oceanic Technol.*, **17**, 130–139.

Market, P. S., R. W. Przybylinski, and S. M. Rochette, 2006: The role of sublimational cooling in a late-season midwestern snow event. *Wea. Forecasting*, **21**, 364–382.

Marwitz, J., and J. Toth, 1993: The Front Range blizzard of 1990. Part I: Synoptic and mesoscale structure. *Mon. Wea. Rev.*, **121**, 402–415.

Meteorological Education (MetEd), cited 2013: Topics in precipitation type forecasting. [Available online at www.meted.ucar.edu/norlat/snow/preciptype/.]

National Center for Atmospheric Research (NCAR), cited 2013: The radar bright band. [Available online at www.eol.ucar.edu/homes/rilling/rad_ex/brightband/bright_band.html.]

NWS, cited 2013: Winter Statistics – Huntsville. [Available online at www.srh.noaa.gov/hun/?n=winterstatisticsforhuntsvilleandmuscleshoals.]

Petersen, W. A., and Coauthors, 2005: The UAH-NSSTC/WHNT ARMOR C-band dual-polarimetric radar: A unique collaboration in research, education and technology transfer. Preprints, *32nd Conference on Radar Meteorology*, Albuquerque, NM, Amer. Meteor. Soc., 12R.4. [Available online at ams.confex.com/ams/pdfpapers/96524.pdf.]

Ryzhkov, A. V., and D. S. Zrnić, 1998: Discrimination between rain and snow with a polarimetric radar. *J. Appl. Meteor.*, **37**, 1228–1240.

Stewart, R. E., and P. King, 1987: Freezing precipitation in winter storms. *Mon. Wea. Rev.*, **115**, 1270–1279.

Straka, J. M., D. S. Zrnić, and A. V. Ryzhkov, 2000: Bulk hydrometeor classification and quantification using polarimetric radar data: Synthesis of relations. *J. Appl. Meteor.*, **39**, 1341–1372.

Thurai, M., V. N. Bringi, L. D. Carey, P. Gatlin, E. Schultz, and W. A. Petersen, 2012: Estimating the accuracy of polarimetric radar–based retrievals of drop-size distribution parameters and rain rate: An application of error variance separation using radar-derived spatial correlations. *J. Hydrometeor.*, **13**, 1066–1079.

Warning Decision Training Branch (WDTB), cited 2013: Introduction to the top-down methodology. [Available online at www.wdtb.noaa.gov/courses/winterawoc/IC6/lesson1/player.html.]

Zrnić, D. S., N. Balakrishnan, C. L. Ziegler, V. N. Bringi, K. Aydin, and T. Matejka, 1993: Polarimetric signatures in the stratiform region of a mesoscale convective system. *J. Appl. Meteor.*, **32**, 678–693.